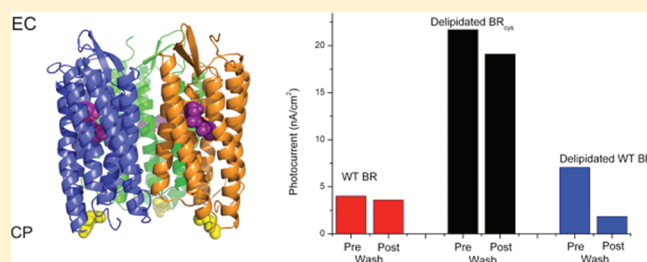


Enhanced Photocurrent in Engineered Bacteriorhodopsin Monolayer

Amol V. Patil,[†] Thenhuan Premaruban,[†] Olivia Berthoumieu,[‡] Anthony Watts,^{*,‡} and Jason J. Davis^{*,†}[†]Physical and Theoretical Chemistry Laboratory, Department of Chemistry, University of Oxford, South Parks Road, Oxford OX1 3QZ, U.K.[‡]Department of Biochemistry, University of Oxford, South Parks Road, Oxford, OX1 3QU, U.K.

S Supporting Information

ABSTRACT: The integration of the transmembrane protein bacteriorhodopsin (BR) with man-made electrode surfaces has attracted a great deal of interest for some two decades or more and holds significant promise from the perspective of derived photoresponse or energy capture interfaces. Here we demonstrate that a novel and strategically engineered cysteine site (M163C) can be used to intimately and effectively couple delipidated BR to supporting metallic electrode surfaces. By virtue of the combined effects of the greater surface molecular density afforded by delipidation, and the vicinity of the electrostatic changes associated with proton pumping to the transducing metallic continuum, the resulting films generate a considerably greater photocurrent density on wavelength-selective illumination than previously achievable with monolayers of BR. Given the uniquely photoresponsive, wavelength-selective, and photostable characteristics of this protein, the work has implications for utilization in solar energy capture and photodetector devices.



INTRODUCTION

Bacteriorhodopsin (BR) is a stable transmembrane photoactive chromoprotein found in *Halobacterium salinarium*. BR, in its native state, exists as purple membrane (PM) patches consisting of BR molecules and lipids (in a ratio of 3:1 by mass) arranged in a 2D hexagonal crystalline lattice.¹ Within these membranes the protein is trimeric with each monomer, an independent proton pump composed of seven transmembrane helices. The central region of each monomer is occupied by a retinal chromophore covalently bound via a Schiff base to a lysine residue on the G helix.² The monomeric protein itself is made up of 248 amino acids and has a mass of 26 kDa.³ In its dark adapted state the protein exists as two conformers in a 1:1 mixture,^{4,5} all-*trans* BR₅₆₈ and the 13-*cis* BR₅₄₈. Spectroscopic and crystallographic studies show that the photoactive retinal is embedded in a well-characterized environment, with considerable electron delocalization throughout the retinal and neighboring binding site aromatic residues.^{6,7}

Upon illumination with light in the 500–650 nm range ($\lambda_{\max} \sim 570$ nm)⁸ the central retinal chromophore absorbs a photon which initiates a conformational change from the all-*trans* to the 13-*cis* retinal state, the first step in a photocycle resulting in the translocation of a proton from the cytoplasmic side of the membrane to the extracellular, a process in which the Schiff base and Asp85 and Asp96 play a central role.^{9,10} Within this photocycle the protein moves through a number of spectrally distinguishable quasi-stable states (K, L, M, N, and O). The first step of this cycle, the formation of K₅₉₀, is the only one that requires energy; the remaining steps are a sequence of thermal relaxations that return the retinal to its all-*trans* conformer.⁴ The retinal

isomerization occurs within a few picoseconds of the photocycle initiation and changes the position of the Schiff base by ~ 0.4 Å.^{11,12} Even though this charge redistribution induces both an internal photovoltage within ns of illumination¹³ and a significant change in the spectral properties of BR (λ_{\max} changes from 568 to 412 nm),¹⁴ it results in a relatively minor conformational change (concentrated mainly in the orientation of helices F and G).¹⁵ Here, the M163C mutation on the E-F loop of BR has been designed to exploit this sensitivity, that is to bring the most responsive part of the protein into close proximity to the underlying surface.

Wild-type BR, which occurs as a two-dimensional crystal, exhibits exceptional thermal and photostability; indeed it is thermally stable at 120 °C for several days¹⁶ and possesses a photostability that vastly exceeds that of synthetic analogues (and greatly increases potential application).^{17,18} These characteristics have driven a considerable interest in the incorporation of BR into electronic circuitry; suggested applications have included an artificial retina, photochromic data storage, holographic cameras, and information processing.^{13,14,19,20}

A diverse range of methods for immobilization of BR have been explored and documented. These have included drop drying, which results in nonorientated multilayers;²¹ Langmuir–Blodgett approaches, in which films are initially compressed at an air–water interface;²² the use of electrophoretic sedimentation (wherein external electric fields act on the purple membrane

Received: November 2, 2011

Revised: December 5, 2011

Published: December 08, 2011

dipole moments) to generate orientated mono/multilayers;²³ antibody mediated oriented immobilization;²⁴ host guest mediated immobilization;²⁵ and encapsulation in polymeric or sol gel based supports.^{26,27} Such assemblies have been typically characterized with surface probe microscopy^{28–30} and electron microscopy,^{31,32} though often only poorly.

Though photocurrents have been detected in BR films for perhaps 25 years, they are multicomponent in nature and have been the subject of conflicting assignments and proposed mechanistic origin. Despite the fact that initial hypotheses suggested photoinduced intramolecular charge displacements (pH independent) as the cause of photocurrent,²⁴ it is likely that the typically measured response, those outside of the picosecond regime,³³ is associated with proton discharge from the extracellular surface as the BR photocycle moves to the M state.^{34–37}

The vast majority of interfacial photocurrent analyses have employed an optically transparent indium tin oxide surface^{19,22,32,35,38,39} with, additionally, some precedence for immobilization on metallic films^{8,40–43} and model membranes.⁴⁴ Attempts to enhance the photocurrent by codeposition of quantum dots (activated by same optical wavelength as BR)^{45,46} or silver nanoparticles (to augment the photoinduced current by forcing BR molecules to follow a shorter photocycle and thus increase the rate of proton release) have also been reported.⁴⁷ Significantly, under conditions of moderate (<1 V) bias, current densities per monolayer are typically in the pA regime.⁴⁸

Here, we have sought to generate highly controlled and orientated BR monolayers on gold electrodes in which surface density is increased by removing the protein from the confines of the normally used “purple membrane patches” through partial delipidation, and then utilizing the orientated chemisorption afforded by a single solution exposed surface cysteine. BR has no indigenous cysteine residues. By strategically replacing a methionine residue on the conformationally sensitive EF loop of BR with a cysteine, the cytoplasmic face of the receptor is chemically anchored to a gold substrate, with up to three anchor points per trimer, as depicted in Figure 1. It was anticipated that these combined effects would not only increase functional surface coverage but also maximize the degree to which any internal or surface localized electrostatic changes are detected by the transducing circuitry. Statistical data have been collected for a large number of wild-type (lipidated and delipidated) and mutant (delipidated) samples to demonstrate enhanced photocurrent and photoswitching of BR in this novel configuration.

MATERIALS AND METHODS

All chemicals were reagent grade (Sigma Aldrich) and were used without further purification. Deionized water (18.2 M Ω cm⁻¹) (Millipore Ltd.) was used throughout.

Transparent Electrodes. Thin gold films (2 nm of Chromium as adhesion layer, 10 nm of gold), to be used as working electrodes, were prepared by evaporating on glass coverslips (#0, 0.08–0.11 mm thick, Menzel Glasser). ITO coated glass (0.14 mm thick, 100 Ω /cm², Diamond Coatings Ltd.) was used as a counter electrode. Electrodes (Gold & ITO), prior to use, were cleaned in freshly prepared piranha solution (*Caution: Piranha is a very strong oxidizing agent which will react violently with any organic material and must be handled with extreme care.*)

BR Samples. Wild-type and BR_{cys} mutant were grown in peptone medium and purified following standard procedures⁴⁹ (M163C BR_{cys} mutant was originally provided by Prof. Turner, University of Miami, School of Medicine, USA). Stock solutions

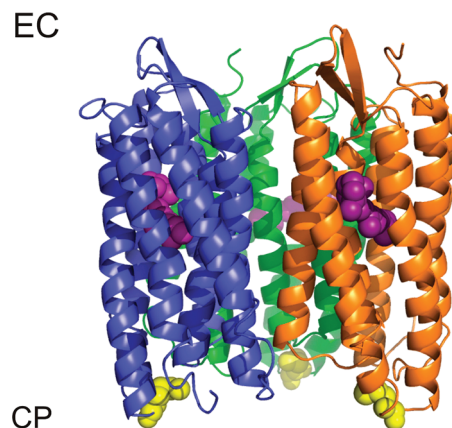


Figure 1. Ribbon representation of BR trimer (PDB: 1BRR) shown with the retinal and mutation sites highlighted (the methionine residue at the 163rd position of the cytoplasmic side (CP) of the protein is replaced with a cysteine; shown as yellow spheres). This mutation is present three times for each BR trimer.

were diluted using 18.2 M Ω cm⁻¹ deionized water. Experiments typically utilized 50 μ L aliquots which had been shaken prior in a Grant Bio Vortex for 2 min to ensure dispersion.

Retinal bleaching was achieved by adding 0.2 M hydroxylamine (pH 7.0) to the delipidated BR sample and stirring under a halogen lamp. The purple color faded away within 30 min. The sample was then centrifuged and washed several times with deionized water in order to remove hydroxylamine and retinal oxime.

The delipidation process involved native BR overnight incubation in CHAPS detergent, dissolved in 5 mM sodium acetate buffer (pH 5.5), under gentle stirring. Through this process only the lipids which reside outside of the BR trimers were removed, thus breaking down the membrane structure. Those that remained occupy the region within the trimer and are needed to maintain its structure.^{50,51} It should be noted that, after delipidation in acetate buffer, BR samples were extensively washed in 18.2 M Ω cm⁻¹ deionized water. It has been shown previously that removal of these external lipids has little effect on the maximum absorption of the BR molecules, with a shift of \sim 10 nm.⁵²

BR Layer Formation. Within the assembly of the photocell (see below), 50 μ L of 10–20 μ M BR (wild-type/delipidated wild-type/delipidated BR_{cys}) solution were pipetted onto the working gold electrode surface. Controlled submonolayers were generated by placing the photocell, overnight, in a humid light proof box at 4 $^{\circ}$ C. Before use, the remnant BR solution was removed and the working electrode was repeatedly rinsed with deionized water (in order to remove any weakly bound protein). This protocol (termed “solution deposition”) was used also used in a multiple iterative manner (i.e., solution deposition, surface washing, solution deposition) to investigate the possibility of incremental coverage increase.

Photocurrent Measurements. All photocurrent analyses were carried out with a home-built photocell consisting of two optically transparent electrodes (a transparent gold film on a glass working electrode with a transparent gold or ITO counter/reference) between which the BR film and electrolyte solution were sandwiched (see Figure S1). The two electrodes were first cleaned in piranha solution for 10 s and then washed with ethanol followed by deionized water, before being dried under nitrogen. A silicone spacer (1 mm thickness) with a through hole (4 mm radius) was then placed onto the working transparent

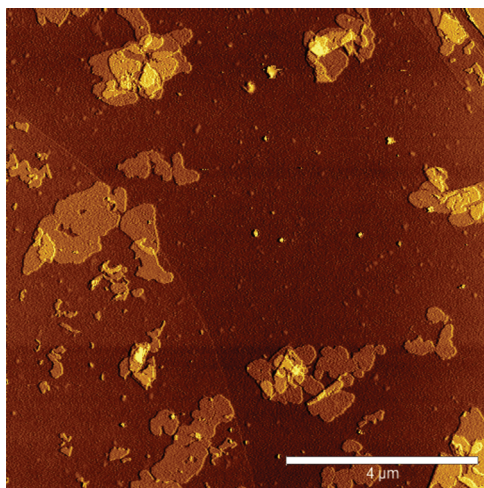


Figure 2. Randomly arranged isolated wild-type purple membrane patches, showing sparse coverage ($\sim 8\text{--}40\%$), adsorbed on a working electrode (evaporated thin gold film on glass), imaged by Atomic Force Microscopy (ambient Tapping Mode at room temperature). Both single and multilayer regions are characteristically present ($20\ \mu\text{M}$ solution, incubated overnight, rinsed in deionized water, and blown dry with nitrogen).

gold electrode, and the desired BR solution was then pipetted in. After the requisite incubation (single/iterative overnight “solution deposition”) the O-ring was backfilled with an electrolyte solution of $100\ \text{mM}\ \text{Na}_2\text{SO}_4$ in $10\ \text{mM}\ \text{PBS}$, pH 7.1 and the cell was sealed with the second electrode (either ITO or transparent gold). The PBS used in all photocurrent analyses was taken from a prepared stock solution. For all photocells aluminum foil was attached to each electrode using silver conductive paint to create electrical contacts. Photocurrent measurements were carried out using an Autolab Potentiostat in chronoamperometric mode (i.e., stepping from an open circuit to the specified bias and then measuring current changes) with subsequent data analysis with integrated GPES (AUTOLAB) or Origin (OriginLab) software. The light source used to illuminate the photocell was an M-150 FibreLite with a 150 W halogen bulb. The two filters used were a 495 nm long pass filter (yellow light) and a 325 nm short pass filter (blue light), the latter of which was used for control purposes. Measurements were carried out in a Faraday cage in order to reduce the amount of electrical noise and to block out any external light. The beam of light was chopped using a home-assembled compact optical shutter, consisting of a rotating disk driven by a battery powered motor. The frequency and time period of illumination were controlled by altering the speed of disk rotation. In each scan the current was measured over a 30 s time period, with a sampling time of 0.05 s. In order to remove small 50 Hz noise contributions, raw data were filtered prior to further analysis. All photocurrents are reported as their peak amplitudes. All BR samples were prepared by incubation in the dark overnight and then were briefly equilibrated under ambient light, as the photocell was constructed prior to photoirradiation and photocurrent analyses under yellow light within an otherwise dark Faraday cage. There was no attempt to further light adapt any BR samples by active illumination prior to such analyses.

Atomic Force Microscopy. Ambient tapping mode atomic force microscopy (TMAFM) imaging was carried out with tapping mode tips (TAP300, nominal resonant freq: 300 kHz, force constant: 40 N/m, BudgetSensors) on a Multimode microscope

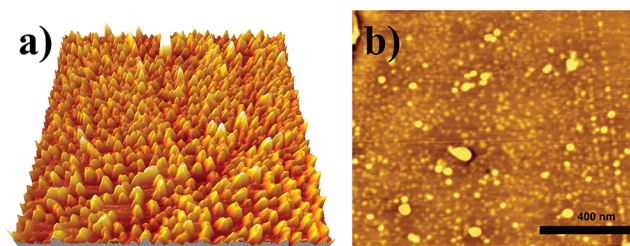


Figure 3. (a) A 3D representation (z scale $0\text{--}3\ \text{nm}$, xy scale $280\ \text{nm}$) of the AFM resolved surface topography of a delipidated BR_{cys} on a gold electrode generated from an overnight solution phase deposition in a $20\ \mu\text{M}$ solution. The sample was subsequently rinsed with deionized water and blown dry prior to imaging in air. The smallest resolved features, $20\text{--}30\ \text{nm}$ in diameter and $1\text{--}1.5\ \text{nm}$ height, are assigned to single isolated BR_{cys} trimers. The molecular density characteristic of these films is clear, unprecedented, and reproduced over large areas (as shown in (b) scale bar: $400\ \text{nm}$).

(Digital Instruments, Ltd.) in conjunction with a Nanoscope IV control system. A J scanner was used, with lateral ranges of $\sim 125\ \mu\text{m}$. Images were imported into and analyzed from Gwyddion (open source software which can be found at <http://gwyddion.net/>) or Scanning Probe Image Processor (Image Metrology) software packages.

RESULTS AND DISCUSSION

The surface assembly of proteins and enzymes on electrode surfaces can be characterized at molecular levels of spatial resolution by scanning probe methods, and indeed surface assembled purple membranes have been routinely imaged in the past on a variety of substrates.^{53,54} AFM imaging herein of cleaned evaporated gold surfaces (rms roughness $1.1\ \text{nm}$) exposed to dilute solutions of wild-type BR showed clear evidence of patches which ranged from a few tens to hundreds of square nanometers (Figure 2) with typical coverage ranging from 8% to 40% ($20\ \mu\text{M}$ solution incubations varying from 1 hour to overnight) of the available surface. Upon removal of the lipid from the purple membrane (wild-type and mutant), the individual trimers were released. With the mutant BR_{cys} protein this leads to molecular films dominated by chemisorbed isolated trimer entities which are tip convoluted with topographical sizes in the 20 to $40\ \text{nm}$ range with an average height of $\sim 1.5\ \text{nm}$ (Figure 3). A topographical analysis of delipidated wild-type films, where the protein–surface association lacks the stability conferred by either a cysteine–gold bond (the mutant) or a large surface area of interaction (native purple membrane), showed only very sparse trimer coverage, but it was possible only with difficulty. Analyses of delipidated BR_{cys} samples resolved, strikingly, fairly homogeneous monolayers of high molecular density ($70\text{--}80\%$ as calculated using Gwyddion SPM analysis software). Significantly, membrane patches *are not observed* in either of the delipidated samples.

The thiolate chemisorption active with the M163 mutant could be further confirmed and quantified by reductive stripping voltammetry. Specifically, in sweeping the surface potential of the underlying electrode cathodically in $100\ \text{mM}\ \text{NaOH}$, a reduction peak at $\sim -1.1\ \text{V}$ vs SCE originating from cleavage of the gold–thiolate bonds is detected (see Figure S2; such stripping peaks are not observed in control experiments with the wild-type BR). An integration of this cathodic current produces a surface coverage value of $\sim 5.3\ \text{pmol}/\text{cm}^2$ ($\sim 80\%$ coverage, with

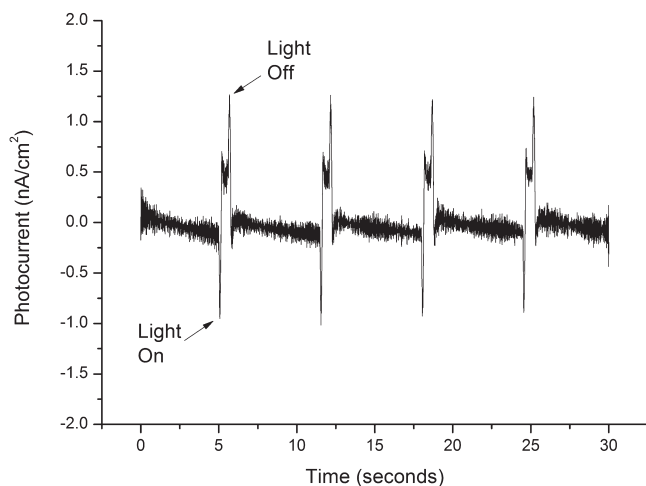


Figure 4. Transient photocurrent responses, coincident with shutter frequency, as observed for a typical randomly orientated wild-type BR sample (overnight solution deposition from 20 μM stock) on an optically transparent gold electrode (0.5 cm^2) at 100 mV bias, under $77\text{ W}/\text{cm}^2$.

a 34 nm^2 footprint for each trimer⁵⁵), which is in excellent agreement with AFM observations. The anchoring role of the solution exposed cysteine residue was additionally evident in comparative analyses of layer mechanical stability (see photocurrent analyses below).

To summarize, then, delipidation and mutagenesis of BR enables robustly chemisorbed and orientated dense molecular films to be formed on pristine gold electrodes.

Comparative Layer Photoresponse. With all prepared BR adlayers, under an appropriate voltage bias, a surface illumination within 500–650 nm light results in transient cathodic and anodic photocurrent, the origins of which we attribute to polarization of the underlying working electrode resulting from localized pH changes.^{35,56} Specifically proton release during the first stages of the BR photocycle leads to a sudden drop in the local pH within the monolayer region. This results in an anodic polarization of the underlying electrode, which, under potentiostatic control, generates a cathodic capacitive current transient.⁵⁶ When the light source is turned off reprotonation of the BR cytoplasmic side from the solution leads to a pH increase, a cathodic polarization, and the resulting anodic capacitive transient (Figure 4).

It is noteworthy that we are assigning the origin of these currents specifically to electrostatic changes caused by the accumulation or depletion of protons within the Debye layer. That an estimation of this layer thickness ($<1\text{ nm}$ predicted by a Gouy–Chapman model) lies well within the BR molecular height ($\sim 5\text{ nm}$) is suggestive of significant and very rapid proton diffusion into/out of this zone through the photocycle.

Control experiments with equivalently prepared photocells *without* BR (or with bleached, retinal-free, i.e., nonphotoresponsive BR: see Figure S3) show small anodic stationary currents which we attribute to a photoelectrochemical response of gold oxide (see Figure 5a).⁵⁷ This current scales with light intensity and applied bias with typical maximal values ($\sim 5\text{ nA}/\text{cm}^2$ at 500 mV bias and light intensity of $77\text{ W}/\text{cm}^2$) significantly lower than BR photocycle ascribed transient peak photocurrents under equivalent conditions ($\sim 20\text{ nA}/\text{cm}^2$). It is, further, possible to deconvolute this response from that associated with the BR photocycle (which is also bipolar, more transient, wavelength specific, and highly dependent on the form of BR used) by filtering the

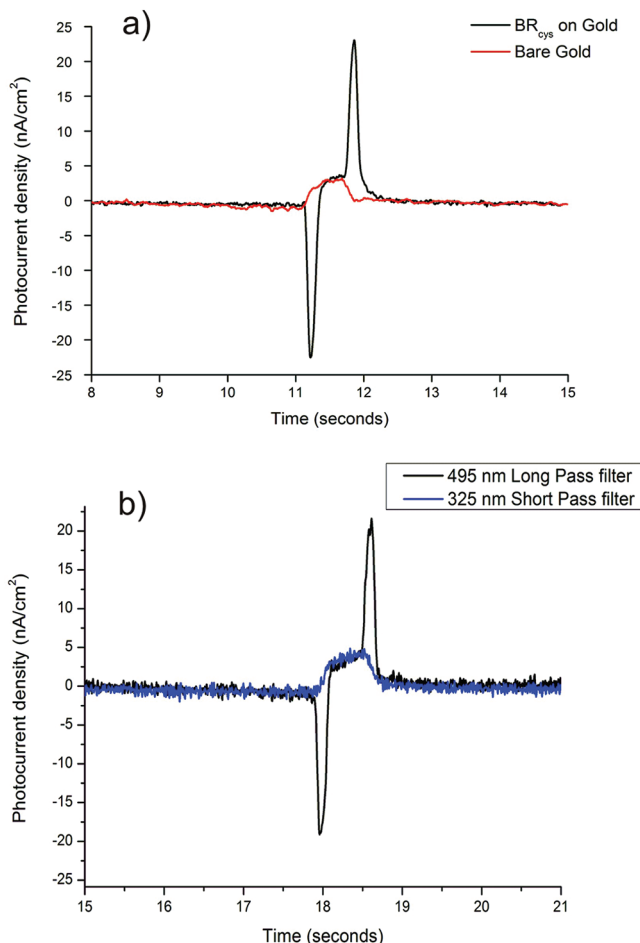


Figure 5. (a) Typical anodic stationary current response of a cleaned transparent gold electrode (with ITO as counter electrode, backfilled with buffer) overlaid with a transient photocurrent response of delipidated BR_{cys} on an equivalent surface (overnight incubation with 20 μM stock solution prior to washing and analysis). (b) Photocurrent response from equivalent BR_{cys} film with and without 325 nm short pass filtering, where it is demonstrably possible to quench the photochemical response of the BR and, then, to confirm the BR photocycle independence of the anodic stationary current. Measurements carried out at voltage bias of 500 mV and $77\text{ W}/\text{cm}^2$.

incident light through a 325 nm short pass filter (which switches off the BR photocycle contributions) as shown in Figure 5.

By tuning the pH of the supporting buffer, it is possible to change the magnitude of the transient peak photocurrent. Specifically, on increasing the solution pH from an acidic starting point, photocurrents are observed to progressively increase, peaking at pH 7.1 and then dropping sharply with a further increase in the pH (see Figure S4). These observations are fully consistent with proton uptake preceding release at low pH (with accumulation of the O state), with, at high pH, proton release occurring before uptake (with an associated accumulation of the N state). These observations are also, of course, further demonstrative of the protic nature of observed current transients.^{58,59}

Specific Effects of Delipidation and Mutagenesis. In order to investigate the effect of the delipidation and mutagenesis on BR photocurrent generation for monolayers generated here by carefully controlled solution deposition, a systematic survey of experimental parameters, namely incident light intensity

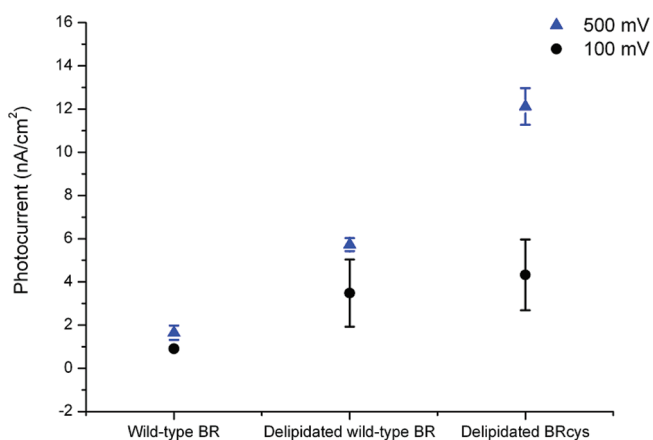


Figure 6. Dependence of transient photocurrent (77 W/cm^2 irradiation) at 100 mV (black circle) and 500 mV (blue triangle) with applied voltage as seen for solution deposited submonolayer films of wild-type/delipidated wild-type and delipidated BR_{cys} (all prepared at $20 \mu\text{M}$) with transparent gold working and counter electrodes. The effects of progressive increase in surface density and electronic coupling which accompany delipidation and chemisorption are clear, as one proceeds from the Wild-type BR to delipidated mutant BR. For some solution deposition experiments transparent gold electrodes were used as counter electrodes resulting in peak transient photocurrents of $\sim 14 \text{ nA/cm}^2$ at 500 mV and 77 W/cm^2 . Upon using ITO counter electrodes (with their higher transmission) peak currents increased to $\sim 23 \text{ nA/cm}^2$ under the same conditions.

($30\text{--}77 \text{ W/cm}^2$) and applied voltage bias (100–500 mV), was carried out.

Photocurrent analyses over ~ 100 samples of wild-type, delipidated wild-type, and delipidated BR_{cys} confirm that current densities increase strikingly with both delipidation ($\sim 300\%$ increase at 100 mV bias compared to wild-type samples) and cysteine mutation mediated chemisorption ($\sim 20\%$ increase of delipidated BR_{cys} mutant over delipidated wild-type). We ascribe this increase in layer photoresponse to the specific effects of increased functional molecular density. For solution deposition (from $20 \mu\text{M}$ BR stock) where sub/monolayers are generated, the packing of wild-type BR (PM) patches on the electrode surfaces is comparatively poor (*despite the fact that the hexagonal packing of trimers within purple membrane patches is highly efficient*¹) (see Figure 2) as compared to that achievable with the delipidated mutant. Delipidation, then, occurs with retention of functionality, frees the protein from the confines of rigid two-dimensional patches, and facilitates a stable, densely packed chemisorption where a solvent exposed cysteine is present. Though delipidation is expected to occur with retention of approximately one-third of the initial lipid (inside the trimer),⁶⁰ the packing density achievable at a solid interface is reflective not only merely of the percentage by volume of sample which is a functional protein but also the effectiveness with which this binds across the surface. We believe, then, that the importance of delipidation lies also within the freedom given to BR trimers to bind effectively across the whole transducing gold surface (the wild type PM patches, due to their rigid “plate” like structure, cannot pack as tightly across the surface; see Figure 2). Since the origin of the triggered photoresponse is electrostatic, currents will be expected to scale with the surface density of functional (proton pumping) molecules as indicated in Figures 6 and 7. For any given incident light intensity or BR sample, photocurrent magnitudes scale

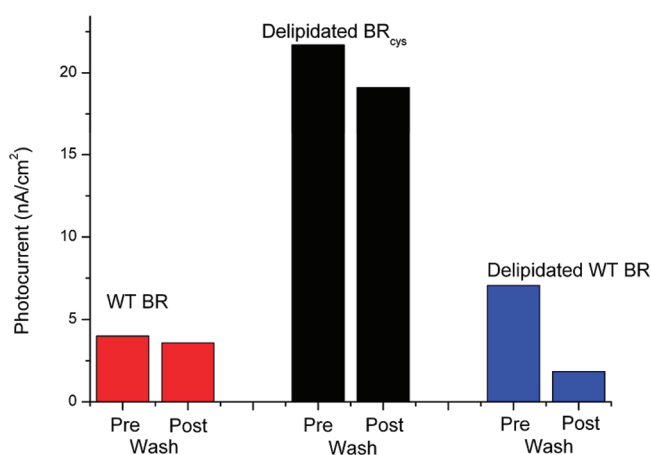


Figure 7. BR molecular films prepared by overnight solution deposition ($20 \mu\text{M}$ for all samples here) exhibit striking difference in levels of both photocurrent and stability. The anchoring role of the mutant cysteine is particularly clear. Wild-type BR films benefit from strong physisorption associated with large PM “patches”. Notable also is the instability of the delipidated wild-type BR films, in which the trimer–surface interaction benefits from neither the large interaction surface of PM nor the anchoring cysteine of the mutant. The higher functional surface density associated with the delipidated BR_{cys} is predictably accompanied by considerably larger photocurrent values in comparison to equivalently prepared wild-type samples. Measurements carried out at a voltage bias of 500 mV and 77 W/cm^2 illumination. A comparison of the mutant protein and current surface densities enables one to derive a photocurrent-per-trimer of the order of 7×10^{-21} amperes. [The error margins associated with accurately quantifying the native BR molecular densities across the entire electrode surface precludes a meaningful equivalent “trimer-level” consideration with these samples.]

rather predictably with applied voltage, with a sensitivity that appears to increase at higher bias (see Figure S5). It is also noteworthy that photocurrents associated with delipidated mutant samples scale most sensitively with applied bias. An examination of the potential reasons for this is currently underway.

The role of the anchoring exposed cysteine residue in facilitating the generation of robust adlayers of highly stable photoresponsive BR is evident in comparative analyses of films prepared from identical concentrations of wild-type, delipidated wild-type, and delipidated mutant BR stock solution; delipidated wild-type BR films are observed to be readily removed from gold surfaces (Figure 7) with a salt/surfactant wash (1 M KCl/1% Tween 20 solution) with no discernible changes in surface density of the delipidated BR_{cys} (an observation consistent with the expected chemical nature of the sulfur–gold association) or wild-type purple membrane (an observation that can be ascribed to the larger surface interaction of the purple membrane with an underlying gold electrode).

A further confirmation of the controlled nature of film formation available through solution phase deposition (overnight incubation at controlled concentration prior to surface washing and photo-cell analyses, with the surface remaining hydrated throughout) is its ability to, stepwise, increase packing efficiency through repeat incubations (at $20 \mu\text{M}$). It is, specifically, observed that current densities for the wild-type and delipidated BR_{cys} films (the mechanical instability of delipidated wild-type films precluded their inclusion in this analysis) initially rise with subsequent depositions prior to tailing off to a plateau as the entire viable electrode surface is occupied (Figure 8). Two points are apparent from such experiments; the first is that the initially higher coverages characteristic of

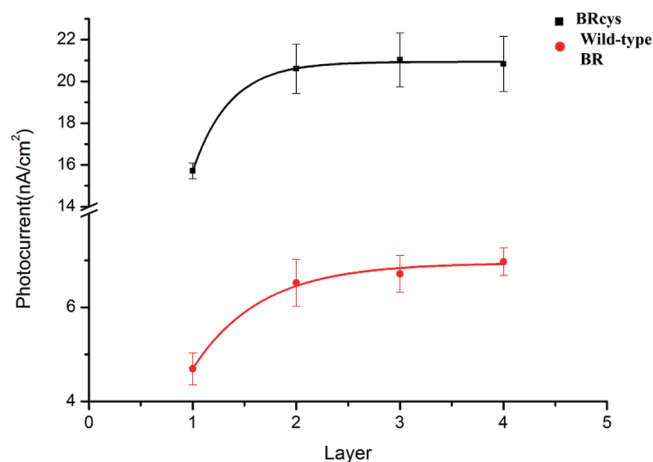


Figure 8. With an iterative application of the solution deposition protocol (here 20 μM) it is possible to study the progression toward a maximum functional surface density for delipidated BR_{cys} (black line) and wild-type BR (red line). Significantly, the current densities (all at 500 mV bias and 77 W/cm²) not only are markedly higher for the mutant films (for reasons as discussed in the main body text) but also plateau after only two incubations (surface coverage being initially ~80%). The initially low surface coverage available with wild-type films continues to increase, typically, through 4 or 5 incubations.

the delipidated BR_{cys} facilitate a more rapid plateau (at just two incubations; see supporting ellipsometric measurements in Figure S6), where photocurrent densities acquired from wild-type films continue to increase up to four or five incubations. The second point is that the functional density attained with the wild-type films remains substantially below that possible with the delipidated BR_{cys} films, reflecting, presumably, the steric, diffusional, and binding advantages of the latter within the film forming and washing processes.

CONCLUSION

The need for a sustainable energy supply needs no further discussion. In natural photosynthetic bacteria, bacteriorhodopsin acts as an exquisitely sensitive and robust, wavelength specific, photoactive proton pump and has been commonly cited as a potential solar conversion, data storage or photoswitching component when integrated with man-made electrodes. As such the photoelectric characteristics of its films have been the subject of extensive study. In nearly all reports to date the protein is native, entrapped within a two-dimensional planar lipid film, and only loosely coupled to transducing electronics. Additionally most of the prior work consists of a relatively poorly characterized monolayer/multilayer on a variety of modified/unmodified electrodes. Where monolayer specific photocurrents have been reported, values range from 3 pA/cm² to, under application of a very high bias, 6 nA/cm².⁴⁸ We have demonstrated, herein, that, in freeing the protein from its associated lipid and introducing a reactive surface cysteine residue, orientated and robust monolayer films can be generated on gold electrodes. Strikingly, this process both retains the protein's exquisite photophysical characteristics and enables a more intimate interfacial sampling of them. The modulated wavelength specific irradiation of these films specifically generates current transients that are reflective of native proton pumping activities. By virtue of the increased molecular surface density afforded by these steps, subsequently observed photocurrent densities are, under moderate bias, some

orders of magnitude greater than those previously reported in films of this type. The robust immobilization of functional delipidated BR trimers across electrode surfaces further enables photoswitching characteristics to be probed at truly molecular scales.⁶¹

ASSOCIATED CONTENT

S Supporting Information. Additional information such as photocell layout, control experiments verifying cysteine bond formation, effect of pH, light intensity. This information is available free of charge via the Internet at <http://pubs.acs.org>.

AUTHOR INFORMATION

Corresponding Author

*E-mail: anthony.watts@bioch.ox.ac.uk; jason.davis@chem.ox.ac.uk.

REFERENCES

- Henderson, R. *J. Mol. Biol.* **1975**, *93*, 123.
- Bridgen, J.; Walker, I. D. *Biochemistry* **1976**, *15*, 792.
- Koyama, K.; Yamaguchi, N.; Miyasaka, T. *Adv. Mater.* **1995**, *7*, 590.
- Jussila, T.; Li, M.; Tkachenko, N.; Parkkinen, S.; L, B.; Jiang, L.; Lemmetyinen, H. *Biosens. Bioelectron.* **2002**, *17*, 509.
- Jin, Y.; Friedman, N.; Sheves, M.; He, T.; Cahen, D. *Proc. Natl. Acad. Sci. U.S.A.* **2006**, *103*, 8601.
- Grigorieff, N.; Ceska, T. A.; Downing, K. H.; Baldwin, J. M.; Henderson, R. *J. Mol. Biol.* **1996**, *259*, 393.
- Hirai, T.; Subramaniam, S.; Lanyi, J. K. *Curr. Opin. Struct. Biol.* **2009**, *19*, 433.
- Choi, H.; Min, J.; Han, K.; Kim, Y.; Lee, W.; Choi, J. *Mol. Cryst. Liq. Cryst.* **2000**, *349*, 303.
- Trissl, H. W.; Montal, M. *Nature* **1977**, *266*, 655.
- Gillespie, N. B.; Wise, K. J.; Ren, L.; Stuart, J. A.; Marcy, D. L.; Hillebrecht, J.; Li, Q.; Ramos, L.; Jordan, K.; Fyvie, S.; Birge, R. R. *J. Phys. Chem. B* **2002**, *106*, 13352.
- Birge, R. *Annu. Rev. Phys. Chem.* **1990**, *41*, 683.
- Prokhorenko, V. I.; Nagy, A. M.; Waschuk, S. A.; Brown, L. S.; Birge, R. R.; Miller, R. J. D. *Science* **2006**, *313*, 1257.
- Xu, J.; Bhattacharya, P.; Váró, G. *Biosens. Bioelectron.* **2004**, *19*, 885.
- Hampp, N. *Chem. Rev.* **2000**, *100*, 1755.
- Hirai, T.; Subramaniam, S. *FEBS Lett.* **2003**, *545*, 2.
- Müller, J.; Münster, C.; Salditt, T. *Biophys. J.* **2000**, *78*, 3208.
- Wang, G.; Porschke, D. *J. Phys. Chem. B* **2003**, *107*, 4632.
- He, T.; Friedman, N.; Cahen, D.; Sheves, M. *Adv. Mater.* **2005**, *17*, 1023.
- Miyasaka, T.; Koyama, K.; Itoh, I. *Science* **1992**, *255*, 342.
- Birge, R. R.; Gillespie, N. B.; Izaguirre, E. W.; Kusnetzow, A.; Lawrence, A. F.; Singh, D.; Song, Q. W.; Schmidt, E.; Stuart, J. A.; Seetharaman, S.; Wise, K. J. *J. Phys. Chem. B* **1999**, *103*, 10746.
- Saga, Y.; Watanabe, T.; Koyama, K.; Miyasaka, T. *J. Phys. Chem. B* **1998**, *103*, 234.
- Miyasaka, T.; Koyama, K. *Thin Solid Films* **1992**, *210–211*, 146.
- Min, J.; Choi, H. J.; Choi, J. W.; Lee, W.; Kim, U. *Thin Solid Films* **1998**, *327–329*, 698.
- Koyama, K.; Yamaguchi, N.; Miyasaka, T. *Science* **1994**, *265*, 762.
- Chen, D.-l.; Lu, Y.-j.; Sui, S.-f.; Xu, B.; Hu, K.-s. *J. Phys. Chem. B* **2003**, *107*, 3598.
- Chen, Z.; Lewis, A.; Takei, H.; Nebenzahl, I. *Appl. Opt.* **1991**, *30*, 5188.
- Weetall, H. H. *Biosens. Bioelectron.* **1996**, *11*, 327.
- Knapp, H. F.; Mesquida, P.; Stemmer, A. *Surf. Interface Anal.* **2002**, *33*, 108.
- Min, J.; Choi, H.; Choi, J.; Lee, W.; Kim, U. *Supramol. Sci.* **1998**, *5*, 687.

- (30) Moller, C.; Allen, M.; Elings, V.; Engel, A.; Muller, D. J. *Biophys. J.* **1999**, *77*, 1150.
- (31) Furuno, T.; Takimoto, K.; Kouyama, T.; Ikegami, A.; Sasabe, H. *Thin Solid Films* **1988**, *160*, 145.
- (32) Miyasaka, T.; Koyama, K. *Chem. Lett.* **1991**, 1645.
- (33) Xu, J.; Stickrath, A. B.; Bhattacharya, P.; Nees, J.; Váró, G.; Hillebrecht, J. R.; Ren, L.; Birge, R. R. *Biophys. J.* **2003**, *85*, 1128.
- (34) Lee, I.; Greenbaum, E.; Budy, S.; Hillebrecht, J. R.; Birge, R. R.; Stuart, J. A. *J. Phys. Chem. B* **2006**, *110*, 10982.
- (35) Robertson, B.; Lukashov, E. *Biophys. J.* **1995**, *68*, 1507.
- (36) Saga, Y.; Watanabe, T.; Koyama, K.; Miyasaka, T. *Chem. Lett.* **1998**, *27*, 961.
- (37) Weetall, H. H.; Samuelson, L. A. *Thin Solid Films* **1998**, 312, 306.
- (38) Wang, J.; Song, L.; Yoo, S.; El-Sayed, M. *J. Phys. Chem. B* **1997**, *101*, 10599.
- (39) Wang, J.; Yoo, S.; Song, L.; El-Sayed, M. A. *J. Phys. Chem. B* **1997**, *101*, 3420.
- (40) Brizzolara, R. A.; Boyd, J. L.; Tate, A. E. *J. Vac. Sci. Technol. A* **1997**, *15*, 773.
- (41) Choi, H.-G.; Min, J.; Lee, W. H.; Choi, J.-W. *Colloids Surf, B* **2002**, *23*, 327.
- (42) Saga, Y.; Watanabe, T. *J. Phys. Chem.* **1999**, *103*, 234.
- (43) Schranz, M.; Noll, F.; Hampp, N. *Langmuir* **2007**, *23*, 11134.
- (44) Horn, C.; Steinem, C. *Biophys. J.* **2005**, *89*, 1046.
- (45) Griep, M. H.; Walczak, K. A.; Winder, E. M.; Lueking, D. R.; Friedrich, C. R. *Biosens. Bioelectron.* **2010**, *25*, 1493.
- (46) Li, R.; Li, C. M.; Bao, H. F.; Bao, Q. L.; Lee, V. S. *Appl. Phys. Lett.* **2007**, *91*, 3.
- (47) Yen, C.; Chu, L.; El-Sayed, M. *J. Am. Chem. Soc.* **2010**, *132*, 7250.
- (48) Jin, Y.; Honig, T.; Ron, I.; Friedman, N.; Sheves, M.; Cahen, D. *Chem. Soc. Rev.* **2008**, *37*, 2422.
- (49) Oesterhelt, D.; Stoeckenius, W. *Methods Enzymol.* **1974**, *31*, 667.
- (50) Jang, D. J.; el-Sayed, M. A. *Proc. Natl. Acad. Sci. U.S.A.* **1988**, *85*, 5918.
- (51) Belrhali, H.; Nollert, P.; Royant, A.; Menzel, C.; Rosenbusch, J. P.; Landau, E. M.; Pebay-Peyroula, E. *Structure* **1999**, *7*, 909.
- (52) Heyes, C.; El-Sayed, M. *Biophys. J.* **2003**, *85*, 426.
- (53) Engel, A.; Gaub, H. E. *Annu. Rev. Biochem.* **2008**, *77*, 127.
- (54) Frederix, P.; Bosshart, P. D.; Engel, A. *Biophys. J.* **2009**, *96*, 329.
- (55) Essen, L.; Siegert, R.; Lehmann, W.; Oesterhelt, D. *Proc. Natl. Acad. Sci. U.S.A.* **1998**, *95*, 11673.
- (56) Saga, Y.; Ishikawa, T.; Watanabe, T. *Bioelectrochemistry* **2002**, *57*, 17.
- (57) Watanabe, T.; Gerischer, H. *J. Electroanal. Chem.* **1981**, *117*, 185.
- (58) Cao, Y.; Brown, L. S.; Needleman, R.; Lanyi, J. K. *Biochemistry* **1993**, *32*, 10239.
- (59) Lu, T.; Li, B. F.; Jiang, L.; Rothe, U.; Bakowsky, U. *J. Chem. Soc., Faraday Trans.* **1998**, *94*, 79.
- (60) Corcelli, A.; Lattanzio, V. M. T.; Mascolo, G.; Papadia, P.; Fanizzi, F. *J. Lipid Res.* **2002**, *43*, 132.
- (61) Berthoumieu, O.; Patil, A.; Xi, W.; Aslimovska, L.; Davis, J. J.; Watts, A. *Nanoletters* **2011**, DOI: 10.1021/nl203965w.